Development of Pulverized Biomass Combustion for Industrial Boiler: A Study on Bluff Body Effect

Niwat Suksam and Jarruwat Charoensuk *

Experimental and numerical investigations were performed for pure pulverized biomass combustion in a 300 kW laboratory swirl burner with a pre-combustion chamber. This work investigated a bluff body at the burner tip and how that affected the combustion characteristics in comparison with a conventional annular orifice burner. The combustion performances were assessed by measuring the temperature distribution in a pre-combustion chamber and furnace, oxygen concentration, and emissions (CO and NO_x). Simulations were carried out and validated, providing insight on flow aerodynamics, particle trajectories, species concentrations, and temperature in a pre-combustion chamber and furnace. It was concluded that the bluff body provided a superior performance in terms of flame attachment and combustion efficiency. However, the emissions were high due to the contribution of thermal NO_x.

Keywords: Pulverized biomass; Swirl burner; Bluff body; Pre-combustion chamber; CFD

Contact information: Department of Mechanical Engineering, Faculty of Engineering, King Mongkut's Institute of Technology Ladkrabang, Bangkok 10520 Thailand;
** Corresponding author: jarruwat.ch@kmitl.ac.th*

INTRODUCTION

Coal consumption has become a debatable issue over recent years because it is a non-renewable resource. The concern regarding the impact of emissions from coal combustion on climate change has increased the interest in biomass as an alternative because it is renewable, considering that it is a carbon-neutral energy resource (Sami *et al*. 2001). However, biomass has lower calorific value because the composition of biomass has a lower carbon content than coal. Additionally, when converting chemical energy to thermal energy *via* combustion, its thermal performance should be considered, *i.e.*, its flame stability, emissions, *etc*.

Pulverized biomass has been adopted for co-firing with pulverized coal in the furnace of an industrial boiler for power generation and process steam. Yi *et al.* (2013) conducted a study with thermogravimetric analysis (TGA) on a blend of ramie residue and coal. The effects of coal blending ratio from 0 to 30 wt% on performance of cyclone furnace were investigated. Ndibe *et al.* (2015) had successfully run a 300 kW combustor firing 100% pulverized torrefied spruce, 100% pulverized coal, and 50% blending of these two types of fuel with pre-heated secondary air at 195 °C. A study using a drop tube furnace was also carried out by Wang *et al.* (2015) on coal and coal-biomass blending combustion performance (coal, straw, and wood). Results suggested a positive effect of blending on combustion efficiency and NO_x emission. The effect of air staging was also evaluated. Aziz *et al*. (2016) had adopted computational fluid dynamics (CFD) for simulation of combustion performance of pulverized fuel blends between palm kernel and coal in an existing power plant. In their study up to 15% of the biomass could be adopted for co-firing without adverse effects on temperature distribution. Darmawan *et al*. (2017) performed experimental and numerical investigation on combustion of hydrothermally treated empty fruit bunch (HT-EFB) blended with coal in a drop tube furnace. A feasibility study was also carried out to integrate fuel processing into power plant system. Pu *et al.* (2017)

recently attempted to use coal blended with biomass as a feedstock for an oxy-fuel bubbling fluidized bed combustor.

The existing plants have not been designed for firing pure pulverized biomass. This is due to the low heating value of volatiles as compared with that from coal, leading to problems with its flame stability. Char burnout was relatively slower due to both a larger biomass particle size and slower reaction kinetics. Firing pure pulverized biomass has been tested in the laboratories of some research institutes.

Ballester *et al.* (2005) carried out experiments on pulverized combustion in a semi-industrial scale furnace with three types of fuel: bituminous coal, lignite, and oak sawdust. Due to the difference in the stoichiometric air ratio of sawdust from coal, the operating conditions for bituminous and lignite were similar; however, there was a significant difference observed for sawdust. The aim of that study was to investigate the effect of different fuel types on some important flame characteristics, such as visible flame shape, distributions of temperature, and some major species (*i.e.*, O_2, CO, NO_x unburned hydrocarbon, and N_2O). It was found that a high volatiles content of lignite led to more intense combustion near the burner when compared with that of the bituminous flame. Such effects were even more prominent in the biomass flame due to it having the highest value of volatiles content. In addition, the results of hydrocarbon concentration and CO concentration confirmed this finding. Therefore, an expanded combustion zone of biomass had been found. However, according to the percentage of unburned carbon 1 m from the burner outlet, the combustion of bituminous particle was the lowest, followed by lignite, and the biomass particles gave the highest percentage of unburned carbon. There were two distinct regions of combustion, with the fist zone exhibiting intense volatiles combustion, followed by the region with trace amounts of delayed volatiles release and the burning of solid char.

Computational fluid dynamics has been widely used for the research and development of a pulverized combustion system. Ma *et al*. (2007) simulated the combustion of biomass in an existing pulverized coal-fired furnace by using a developed CFD model. The prediction showed a reasonable agreement with experimental data. Yin *et al*. (2012) investigated the combustion characteristics when firing pure coal and firing pure wheat straw in a 150 kW swirl-stabilized burner flow reactor under nearly identical conditions. Their results showed dissimilar combustion characteristics between the coal flame and the straw flame. Li *et al*. (2013) investigated the combustion characteristics of pulverized torrefied-biomass firing with high-temperature air by experiment and by simulation using CFD. They reported on the effect of drag force on the devolatilization of biomass and on the flame characteristics. The effect of oxygen concentration in an oxidizer and of air velocity on the flame characteristics were additionally discussed.

Elfasakhany *et al*. (2013) studied the combustion of pulverized biomass by conducting experimental trials and performing a simulation with CFD. There were three groups of particle size distributions ranging from 0.02 mm to 1.2 mm with an aspect ratio greater than 5. The study found a high volatiles release with high concentrations of hydrocarbon and carbon monoxide. The flame resembled a gaseous premixed flame. Three distinctive zones are identified: the preheated zone, the devolatilization zone, and the char oxidation zone. The heat transfer mechanism of the preheated zone for biomass was different from that of the gaseous combustion because the biomass particle was heated up by the radiation mode of heat transfer from the flame and furnace wall prior to undergoing the process of devolatilization. Therefore, pollutant emissions were affected by the burner configuration, particle size, and the furnace chamber. In addition, there was a “rocket effect” during the devolatilization process of the biomass particles.

Weber *et al*. (2015) studied the variety of combustion behaviors in mixed wood, sawdust, fermentation-process residues and grain residues, and South African Middleburg coal. The pulverized coal was injected through an annular nozzle surrounded by the combustion air without swirl, and the biomass was injected through a central pipe nozzle. The furnace was cylindrical with a vertical orientation. The firing rate was 15 kW for all cases. Important flame characteristics such as ignition, temperature rise and distribution, devolatilization, NO_x emission, combustible burnout, fly ash, and slag were investigated. The peak temperature in the volatiles combustion zone when firing coal was 100 °C higher than that of biomass, with an earlier ignition observed for coal. However, all types of fuel fired under this experimental setting achieved a burnout greater than 94.2%. Approximately 50% to 60% of the nitrogen content in sawdust and mixed wood was converted to NO_x, while 16% to 18% was converted for the coal, fermentation-process residues, and grain residues. The bottom ash deposition was found at 950 °C to 1200 °C, and the deposition for the biomass combustion was three times greater than that of the coal combustion.

Karim and Naser (2018) developed user-defined subroutines on a commercial CFD code (AVL Fire) for simulation of woody biomass combustion on moving grate boiler. They found an agreement between the simulation result and the experimental data. Gómez *et al*. (2019) developed a mathematical model for porous media. The model was used together with a commercial software, FLUENT, to simulate combustion, heat and mass transfer in a 35 kW wood pellet furnace. The effect of exhaust gas recirculation (EGR) and excess air was investigated. The model had reasonably represented the phenomena taking place in the reactor.

Elorf and Sarh (2019) found the effect of excess air on the flow aerodynamics and the combustion characteristics of pulverized biomass to be made of olive cake in a vertical furnace with a cylindrical cross section. Fuel was injected radially from the bottom of the furnace to increase the residence time. The study adopted CFD to perform a 3D reacting flow simulation. Biomass with an average particle size of 70 µm was injected radially and combusted under excess air ratios of 1.3, 1.7, 2.3, and 2.7. The simulation suggests that the increase in the excess air ratio would dilute the CO and CO_2 concentrations, decrease the flue gas temperature, and shorten the flame length.

Combustion of biomass in pulverized form has the potential for replacement of conventional fossil fuel. In a conventional burner configuration, fuel is fed into the combustion chamber by pneumatic transport surrounded by combustion air. Introduction of swirl motion to the primary or secondary air stream would help spreading the solid particle around, leading to rapid heat transfer as well as the enhancement of devolatilization and its reaction rate (Zhou *et al*. 2003; Gu *et al*. 2005). However, when combusting biomass with different ignition and char burnout characteristics, additional modification is necessary to improve the combustion performance of the burner.

This paper reports on an achievement made on combustion of pure pulverized biomass with a new burner specifically designed and constructed for pure biomass combustion. The burner is equipped with a pre-combustion chamber, which is used to accommodate ignition of biomass volatile compounds. Apart from the result of the base case, development work is also carried out by installing a bluff body at the burner tip locating at the center of primary air inlet. Discussion is made on how this bluff body affects to the aerodynamics at the central region of a pre-combustion chamber, which leads to improvement of combustion stability and efficiency. The result is verified by temperature distribution and CO emission taken from experiment performed by the authors. CFD is used to investigate aerodynamics, particle trajectories, devolatilization, and combustion when the burner is operated with and without bluff body. Species concentration and NO_x emission are also reported. This simulation enable an in-depth understanding on how the bluff body affects to aerodynamics in the near burner region and eventually to combustion stability and emissions.

EXPERIMENTAL

Experimental Setup

The pulverized biomass swirl burner assembled with a pre-combustion chamber had diameters of 0.385 m and 0.465 m. The furnace had 1 m in inner diameter and 1.215 m in length, as shown in Figs. 1 and 2.

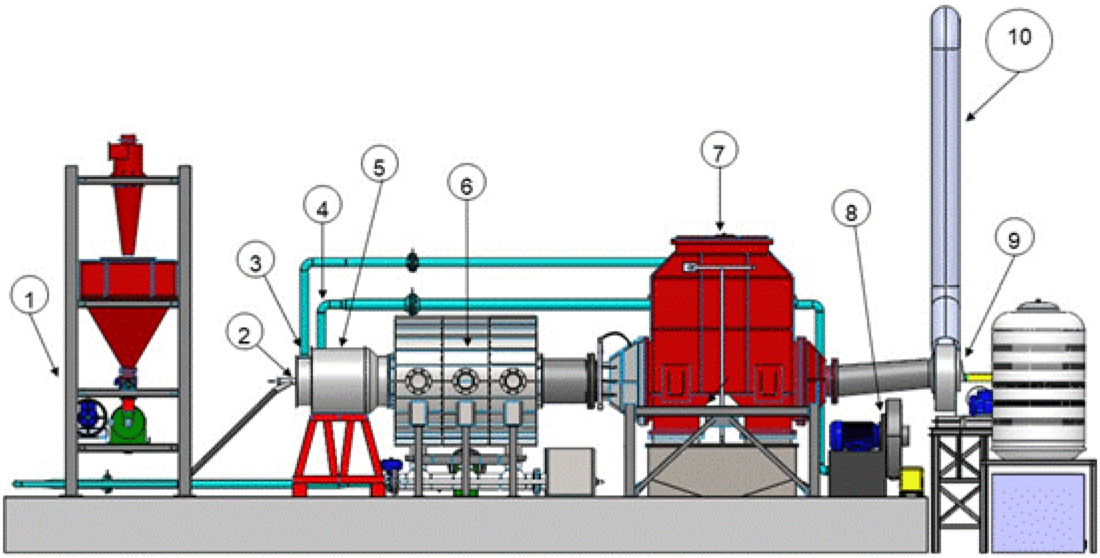

Fig. 1. Pulverized biomass combustion system: (1) pulverized biomass milling and feeding system, (2) primary air and fuel inlet, (3) secondary air inlet, (4) tertiary air inlet, (5) swirl burner and pre-combustion chamber, (6) furnace, (7) flue gas treatment and wet scrubber, (8) air supply system, (9) ID fan, and (10) flue gas stack

Fig. 2. Pulverized biomass combustion burner and furnace

The burner was operated at 300 kW thermal throughput (net) at an equivalence ratio of 0.834 (20% excess air). The fuel and air entered the furnace at 313 K. Primary air and pulverized biomass entered through a central pipe with diameter of 0.0525 m. The primary air and fuel were fed at 0.0186 kg/s and 0.0134 kg/s, respectively. Secondary air travelled through swirl vanes, creating a swirl flow, with a swirl number equal to 0.83, through the annular pipe before entering the pre-combustion chamber at 0.0869 kg/s. Tertiary air entered the furnace from the connector between the pre-combustion chamber and furnace at 0.0334 kg/s, as presented in Table 1. The induced draft (ID) fan was used to draw flue gas from the furnace to the stack. The vacuum outlet of flue gas was controlled at 1500 Pa below atmospheric pressure. The flame temperature was measured using a type K thermocouple with a Yokogawa XL100 Portable Data Station (Yokogawa Electric Corporation, Tokyo, Japan). The combustion gas species were measured using a Testo 330-2 LL flue gas analyzer (Testo AG, Lenzkirch, Germany). The monitoring locations of the pulverized biomass furnace are illustrated in Fig. 3.

Table 1. Operating Conditions of the Furnace

Parameter	Value	Unit
Thermal throughput (based on fuel lower heating value)	300	kW
Pulverized biomass feed rate at primary inlet	0.0186	kg/s
Excess air ratio	1.2	-
Primary air flow	0.0134	kg/s
Secondary air flow	0.0869	kg/s
Swirl number	0.83	-
Tertiary air flow	0.0334	kg/s
Mole fraction of O_2 in air inlet	0.21	-
Mole fraction of N_2 in air inlet	0.79	-
Temperature of primary, secondary and tertiary air inlet	313	K
Outlet vacuum of flue gas	-1500	Pa

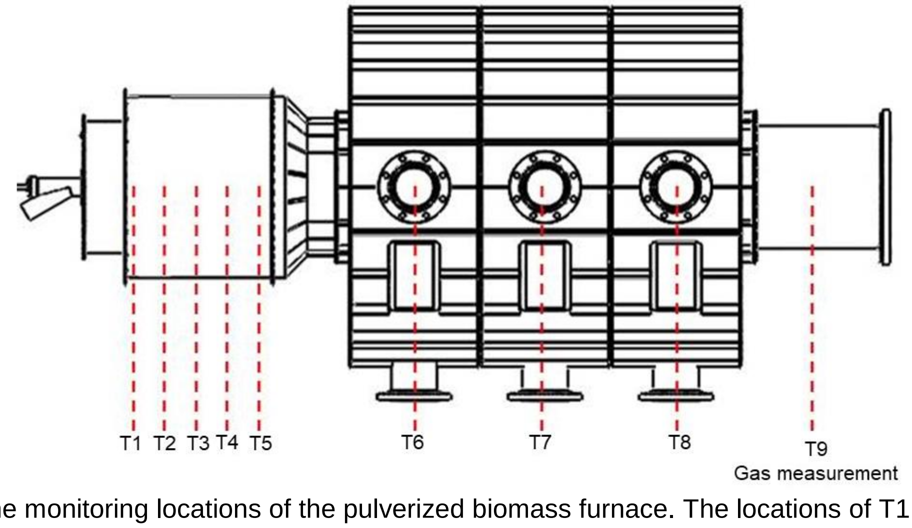

Fig. 3. The monitoring locations of the pulverized biomass furnace. The locations of T1, T2, T3, T4, T5, T6, T7, T8, and T9 have distances from the burner exit as follows: 0.082 m, 0.182 m, 0.282 m, 0.382 m, 0.482 m, 1.081 m, 1.594 m, 2.107 m, and 2.681 m, respectively.

Bluff Body

Two types of nozzles were used. The annular nozzle in Fig. 4a was equipped with a liquefied petroleum gas (LPG) burner at the center of the pipe, resulting in an area ratio of 0.23. A later version (Fig. 4b) was equipped with a 6 mm bluff body with a 45 degree cone angle detached from the LPG burner. This later version provided the blockage ratio of 0.42.

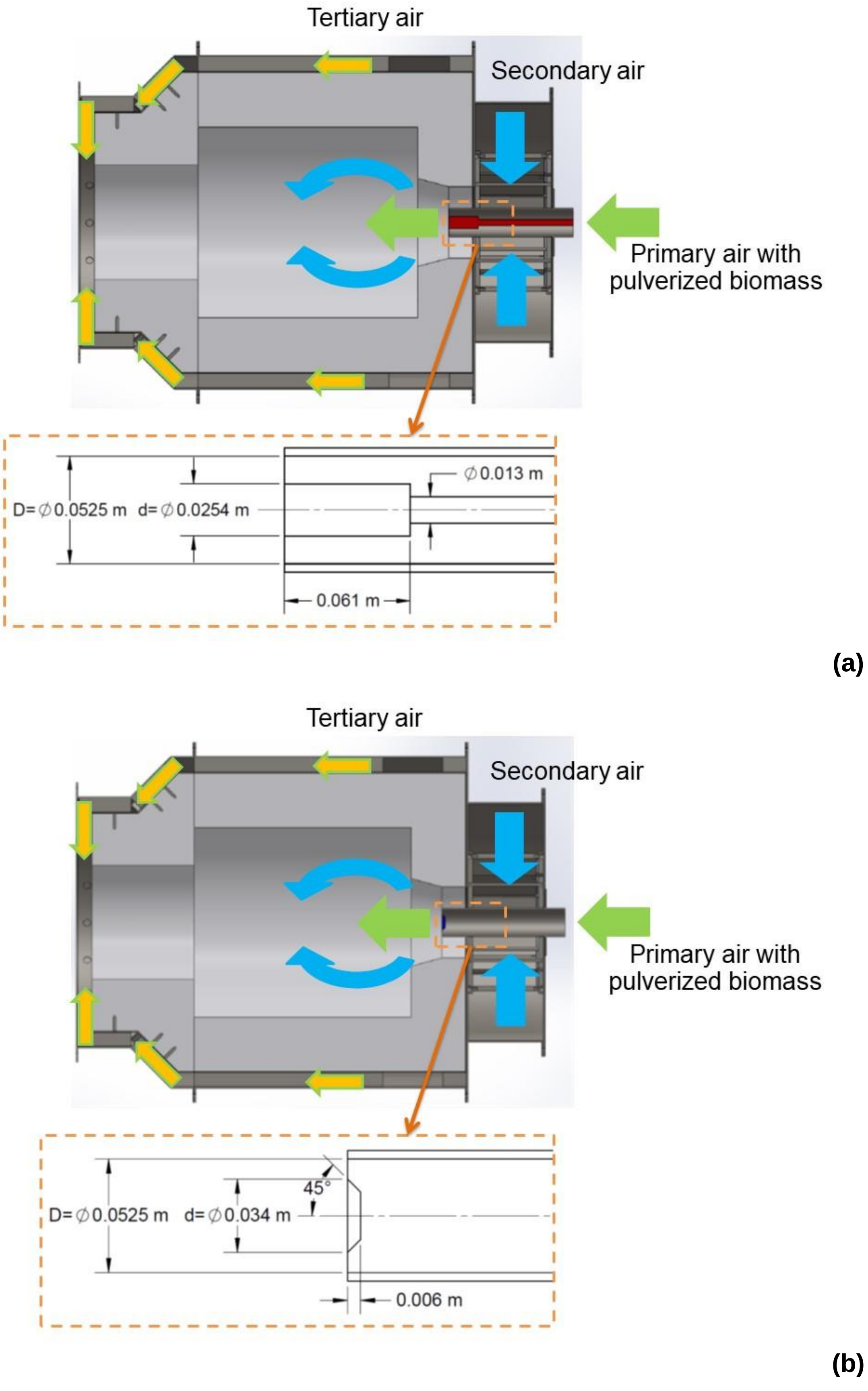

Fig. 4. The two cases of the burner tip in the pre-combustion chamber, with (a) being the annular orfice and (b) being the bluff body

The definitions for the area ratio and blockage ratio (*b.r.*) were similar. It was defined as the cross-sectional area of the no-flow section to the total cross-sectional area of a primary air pipe, as shown in Fig. 4 and Eq. 1,

$$b.r. = \left(\frac{d}{D}\right)^2 \quad (1)$$

where d is the bluff body diameter (m), and D is the primary air pipe diameter (m).

Pulverized Biomass

The pulverized biomass was made from a rubber tree from the southern part of Thailand. Initially, it was pelletized and packed prior to shipment. It arrived at the test site, was pulverized by a hammer mill, and was filtered by a 0.5 mm perforated stainless plate (Fig. 5). The size distribution of the particle after passing through the perforated plate is given in Table 2. The proximate and ultimate analyses of the pulverized biomass are given in Table 3.

(a) **(b)**

Fig. 5. Pulverized biomass fuel, (a) pellet biomass fuel from rubber tree before milling and (b) pulverized biomass fuel after milling

Table 2. Pulverized Biomass Sieve Analysis

Mesh size (µm)	425	300	180	150	75
wt% Passing Through	97.5	80.6	55.1	42.5	24.4

Table 3. Proximate and Ultimate Analysis of Pulverized Biomass Used

Proximate Analysis (wt%, as received)				Ultimate Analysis (wt%, Dry-Ash-Free)						
Ash	Volatile matter	Moisture	Fixed carbon	C	H	O	N	S	HHV (MJ/kg)	LHV (MJ/kg)
2.28	76.68	5.81	15.23	49.42	6.16	43.93	0.49	0	17.50	16.16

HHV: higher heating value; LHV: lower heating value

Mathematical Modeling

The CFD software FLUENT was used to solve the discretized equation of fluid flow combustion, heat and mass transfer, and the tracking of a solid particle. The computational domain of the pulverized biomass combustion furnace is shown in Fig. 6.

The three-dimensional computational domain with a hybrid mesh made with both hexahedral and polyhedral mesh was used. There were approximately 600,000 cells for this simulation. The standard $k-\varepsilon$ model with the standard wall function was used to model the turbulent flow (Launder and Spalding 1974). The radiative heat transfer included in the simulation was the discrete ordinates (DO) model (Raithby and Chui 1990; Chui and Raithby 1993; Murthy and Mathur 1998). The absorption coefficient for radiation was calculated using the weighted sum of gray gas model (WSGGM) (Smith *et al.* 1982; Coppalle and Vervisch 1983).

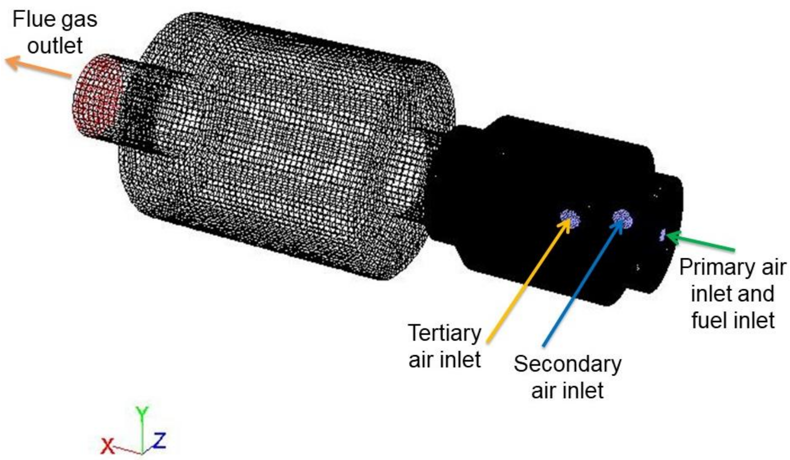

Fig. 6. Computational domain of the pre-combustion chamber and furnace

Discrete phase model

To simulate the pulverized biomass combustion, the discrete phase model (DPM) was adopted using the Eulerian-Lagrangian method. The gas phase was modeled by the Eulerian method, while the discrete solid phase of biomass particles was modeled by the Lagrangian method.

Combustion model

The single kinetic rate model was employed to predict the devolatilization of pulverized biomass (Badzioch and Hawksley 1970). The homogeneous combustion of gas phase was predicted using eddy-dissipation model (Magnussen and Hjertager 1977). The two-step global reaction of the gas phase is modeled in Eqs. 2 and 3.

$$1.04C + 2.32H + 1.04O + 0.013N + 0.58O_2 \Rightarrow 1.04CO + 1.16H_2O + 0.0065N_2 \quad (2)$$

$$CO + 0.5O_2 \Rightarrow CO_2 \quad (3)$$

The char oxidation was determined by the kinetic/diffusion-limited rate model (Field 1969; Baum and Street 1971). The biomass char surface oxidation model is shown in Eq. 4.

$$C(s) + 0.5O_2 \Rightarrow CO \quad (4)$$

Nitric oxides model

In the present work, the nitric oxide (NO_x) model consists of NO_x formation from thermal NO_x, prompt NO_x, and fuel NO_x. In addition, the NO_x reduction from the reburn mechanism was included in the simulation. Thermal NO_x refers to the NO_x formed *via* the high temperature oxidation of the nitrogen of air in the combustion. The rate of thermal NO_x is calculated by the extended Zeldovich mechanism (Zeldovich *et al.* 1947). The prompt NO_x is generated by the reaction between nitrogen and hydrocarbon in a fuel-rich zone of combustion (Fenimore 1971). Fuel NO_x is formed by the reaction between the oxygen and nitrogen contained in the fuel (De Soete 1975). The NO_x reburn mechanism was modeled *via* the reaction of NO_x with HCN to form N_2. Another reaction pathway is between the NO_x and CH_i radicals that formed HCN, which eventually reacts with NO_x *via* the former reaction (Kandamby *et al.* 1996).

Numerical method

The solution methods used for the numerical simulation were the semi-implicit method for pressure linked equations (SIMPLE) for the pressure-velocity coupling scheme, the spatial discretization used the least-squares cell based for gradients, the Pressure Staggering Option (PRESTO!) for pressure, and second order upwind for what remained, *i.e.*, momentum, turbulent kinetic energy, turbulent dissipation rate, gas species, energy, and DO for radiation heat transfer.

RESULTS AND DISCUSSION

Experimental Results

Temperature distribution

Figure 7a shows the temperature distribution in the combustion chamber of the base case having an annular outlet with an area ratio of 0.23. The flame was visualized at a certain distance from the burner outlet, next to the cloud of unburned particles. In contrast, Fig. 7b shows the cone-shaped bluff body with a blockage ratio 0.42, and the suggested attached flame, with a strong illumination of the flame, next to the burner outlet. A relatively greater degree of particle dispersion was observed, implying that the particle could receive more heat transfer from the convection of hot gas and radiation from the refractory of a pre-combustion chamber. In comparison with the annular orifice case, a relatively greater wake region was created next to the bluff body, which was an additional contribution to this effect. These observations agreed with the findings of Liu *et al.* (2016).

Figure 8 shows the axial distribution in temperature. This figure supports the discussion regarding flame attachment as given in an earlier paragraph. The case with a blockage ratio 0.42 provided higher temperatures next to the burner inlet, especially at T2 where the temperature was 497 K higher than that of the same location for the annular orifice case. This indicates there was an earlier ignition. In addition, the furnace temperature was 145 K higher than that of the annular orifice case, implying a higher char reactivity. However, there was small difference in the flue gas temperature at the furnace exit (T9), with a temperature that was 79 K higher than the annular orifice case.

Species concentration

Figure 9 shows the oxygen (O_2) concentration at the furnace exit. The annular orifice case had a greater amount of O_2 left unconsumed, which is logically related to an earlier observation on temperature distribution from Fig. 8.

The carbon monoxide (CO) concentration at the exit plane of the furnace was compared between the base case and the case with a higher blockage ratio, as shown in Fig. 10. The annular orifice had a higher concentration of CO, suggesting there was a lower proportion that burned out. This suggested that the annular orifice nozzle had allowed too much penetration of the primary jet, causing a significant amount of unburned particle to pass through the pre-combustion chamber. These particles when entering the main chamber were quenched by relatively cooler environment. This was unlike the case equipped with a bluff body of blockage ratio 0.42, where a greater portion of the fuel particles had enough residence time to burn in the pre-combustion chamber. This latter case yielded less CO emission at the furnace exit plane.

(a)

(b)

Fig. 7. Flame inside the pre-combustion chamber of the annular orifice (a) and bluff body case (b)

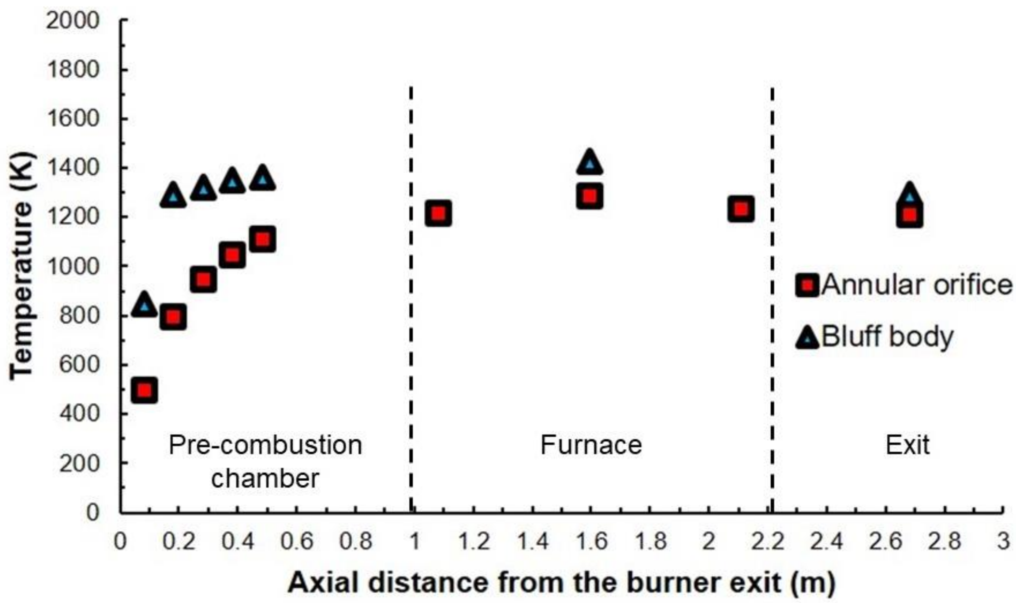

Fig. 8. Axial temperature distribution inside the pre-combustion chamber and furnace

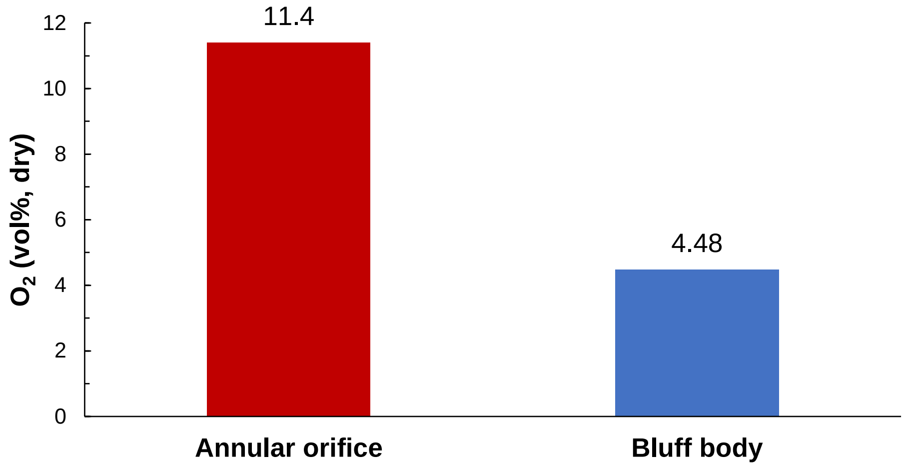

Fig. 9. Oxygen (O_2) concentration (vol%, dry) at flue gas outlet

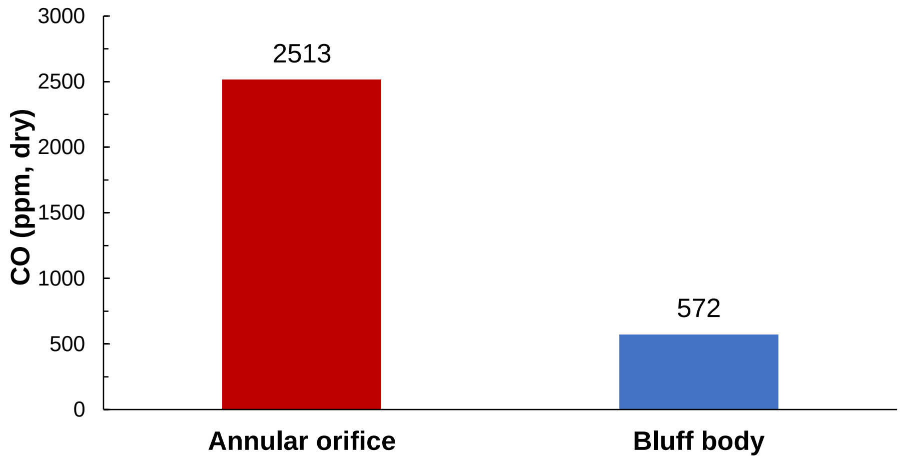

Fig. 10. Carbon monoxide (CO) concentration (ppm, dry) at flue gas outlet

NO_x concentration

Figure 11 shows the comparison of NO_x concentration at the furnace exit. The case with the bluff body with more fuel burn out and a higher flue gas temperature yielded higher NO_x emissions as compared with the annular orifice case. This relationship suggests that NO_x could be attributed to thermal NO_x *via* the Zeldovich mechanism. Although NO_x could come from the reaction involving the nitrogen content in fuel (fuel NO_x), between OH radicals and nitrogen molecules near the flame (prompt NO_x), or other formation pathways, *i.e.*, intermediate N_2O, *etc.*, their contributions to the total NO_x emissions were considered small. For instance, the nitrogen content in fuel accounted for 0.49 wt%, dry ash-free. However, the difference in the NO_x emissions for the annular orifice case was twice as much as the cone-shaped bluff body case.

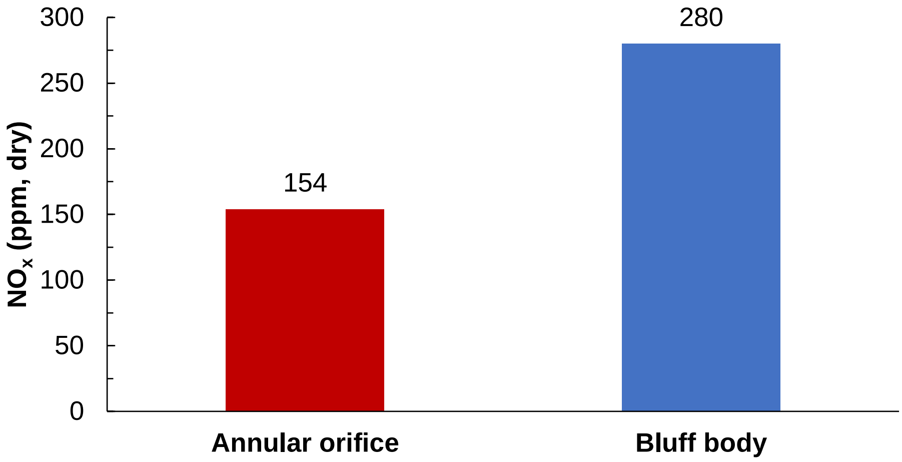

Fig. 11. Nitric oxide concentration (ppm, dry) at flue gas outlet

Model Validation

To obtain a sensible prediction of the numerical results, the model was validated against the experimental results of the bluff body case. Comparisons between the CFD data and the experimental data on the axial temperature profile and species concentrations are shown in Figs. 12 through 15.

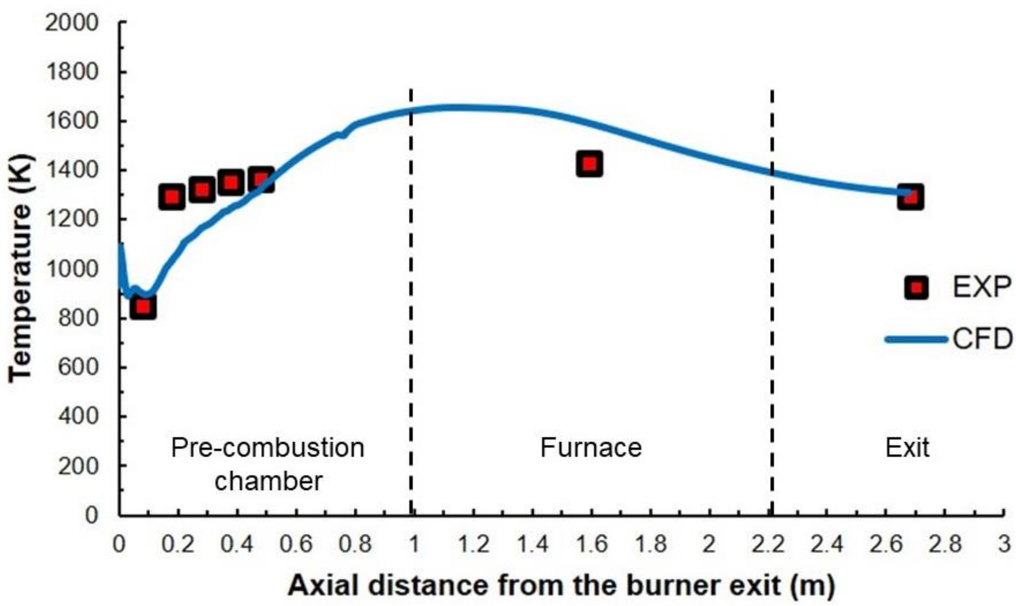

Fig. 12. Comparing axial temperature between CFD and experimental results for the bluff body

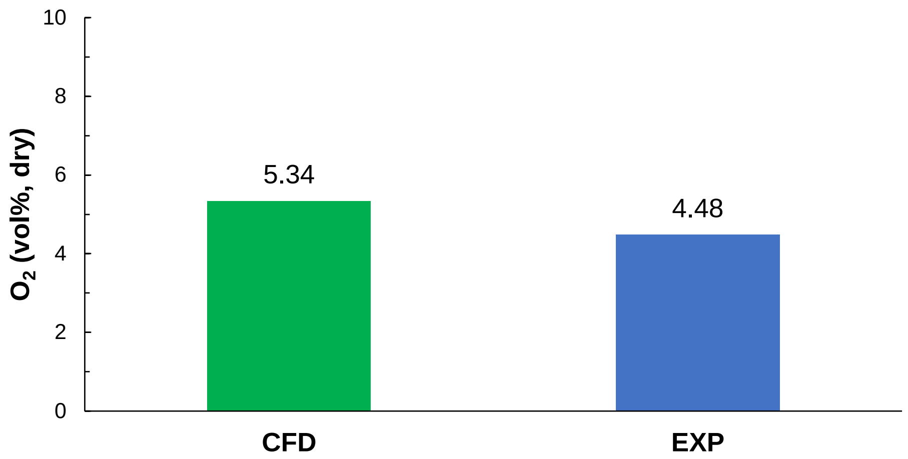

Fig. 13. Comparison of O_2 concentration (vol%, dry) between the CFD and experimental (EXP) results at the flue gas outlet for the bluff-body case

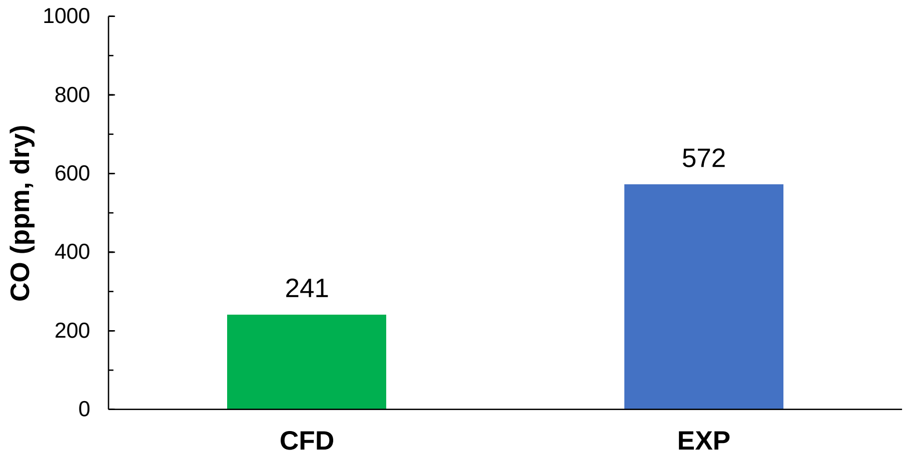

Fig. 14. Comparison of the CO concentration (ppm, dry) between the CFD and experimental (EXP) results at the flue gas outlet for the bluff-body case

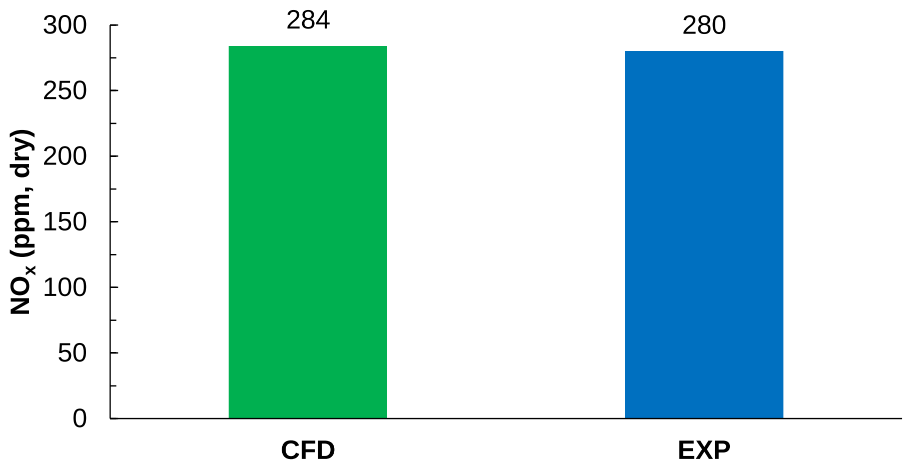

Fig. 15. Comparison of nitric oxide (NO_x) concentration (ppm, dry) between the CFD and experimental (EXP) results at the flue gas outlet for the bluff-body case

The results were generally in agreement because both the experiment and prediction give resembled trends along the axial direction from inlet to the furnace exit plane. However, when focusing on certain locations (*e.g.*, T2, T3, and T4), the prediction provided a slight under-estimation of the flue gas temperature. Nevertheless, the effect caused by the difference in the inlet configuration was reflected in the prediction of the flue gas temperature at T1. The prediction of oxygen concentration at the furnace exit plane was similar to the measured result. However, the model under-predicted the CO concentration when compared with the experimental data. This was due to the fact that the prediction of CO oxidation rate in gaseous phase was defined by the eddy dissipation model, which is based on an assumption of fast kinetics. Development of a CO oxidation model for post combustion zone under an oxygen-depleted environment is an interesting topic of future research, as the reaction rate of CO is more likely to be governed by chemical kinetics. As for the NO_x emissions, the prediction agreed with the experimental results.

Numerical Results

Flow fields

Figure 16 shows the predicted axial velocity component (x-velocity) inside the pre-combustion chamber and furnace. As expected, the case with the annular orifice had a higher magnitude of x-velocity. In the wake region, next to the bluff body, the magnitude of the negative velocity was greater than that of the annular orifice. Moreover, the region with the negative x-velocity value was larger than the annular orifice case. The maximum predicted value in this region was as low as -4.33 m/s for the bluff body case. This effect helped bring the hot flue gas that was downstream of the pre-combustion chamber backward to the region next to the burner exit and promoted volatiles ignition in an "internal recirculation zone." An increase in the flue gas temperature in the pre-combustion chamber caused an increase in the specific volume, thus resulting in a higher flue gas velocity at the connecting port between the pre-combustion chamber section and the main furnace.

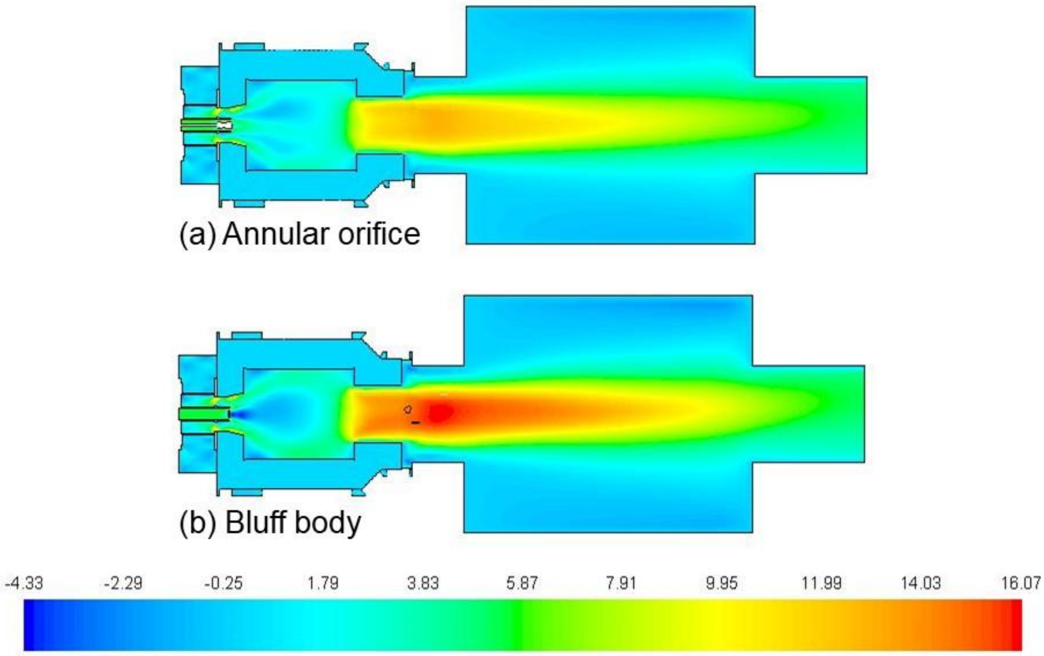

Fig. 16. Axial velocity magnitude (m/s) inside the pre-combustion chamber and furnace for the annular orifice case (a) and bluff body case (b)

Figure 17 illustrates the velocity vector and its magnitude in the pre-combustion chamber. For the annular orifice case (Fig. 17a), the directions of the velocity vectors around the centerline pointed toward the central region of the pre-combustion chamber.

However, the external recirculation zone had a relatively lower magnitude as compared with those found in the case with the nozzle equipped with the bluff body (Fig. 17b). In the latter case, a stronger reverse flow, indicated by the direction of the velocity vectors, pointed backward to the bluff body. In addition, the region of the reverse flow was greater than that of the annular orifice case.

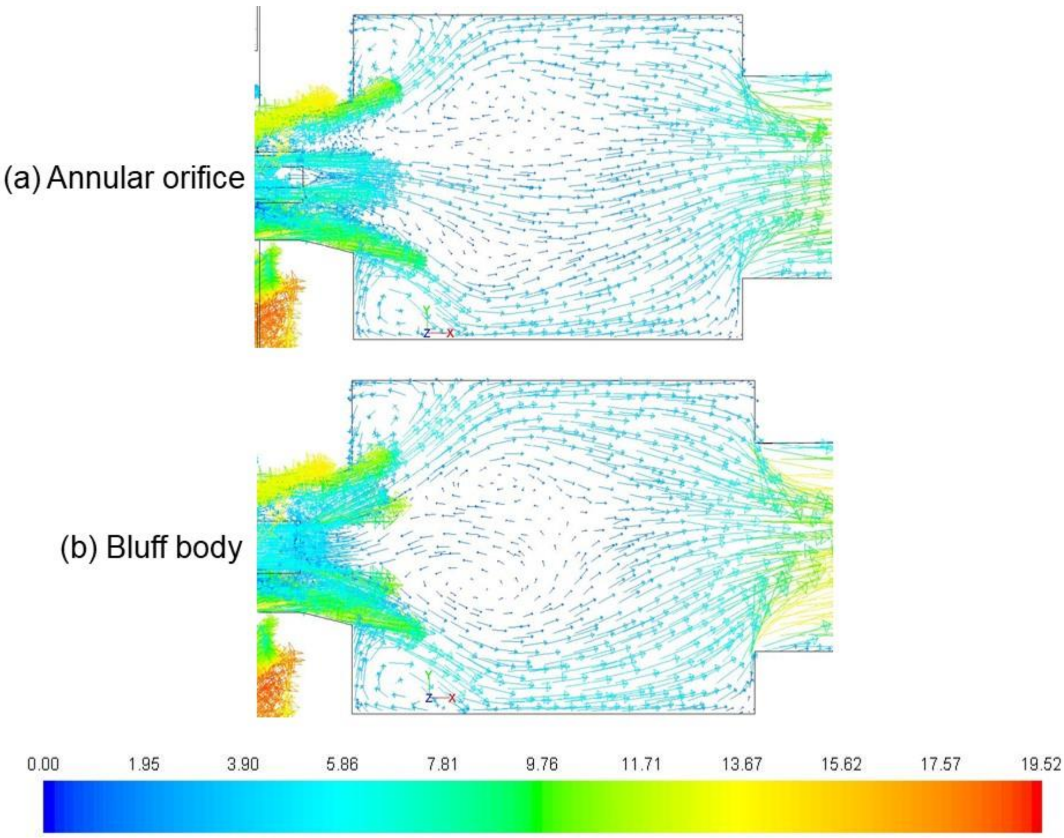

Fig. 17. Velocity vectors colored by the velocity magnitude (m/s) inside the pre-combustion chamber for the annular orifice case (a) and the bluff body case (b)

The particle trajectories of the biomass for both cases are shown in Fig. 18, with different color shades indicating the different levels of volatiles content in the particles. The prediction gives a clear explanation for the experimental data because there was less particle dispersion for the annular orifice case when compared with the bluff body case. This resulted in a relatively poor release of volatiles. For the annular orifice case, volatiles had not completely released from the particle when leaving the pre-combustion chamber (Fig. 18a), while almost all the volatiles had released for the bluff body case. The asymmetry of all the species' concentrations and temperatures discussed in the following sections were due to a gravitational force that brought the particle down toward the lower part of the chamber.

Temperature field

The temperature distribution in Fig. 19 suggests that the bluff body created a high temperature next to it, while a lower temperature value was observed with the annular nozzle. The effect of the aerodynamics that led to this observation was discussed earlier in the experimental results. However, the distribution in the furnace next to the combustion chamber was relatively similar.

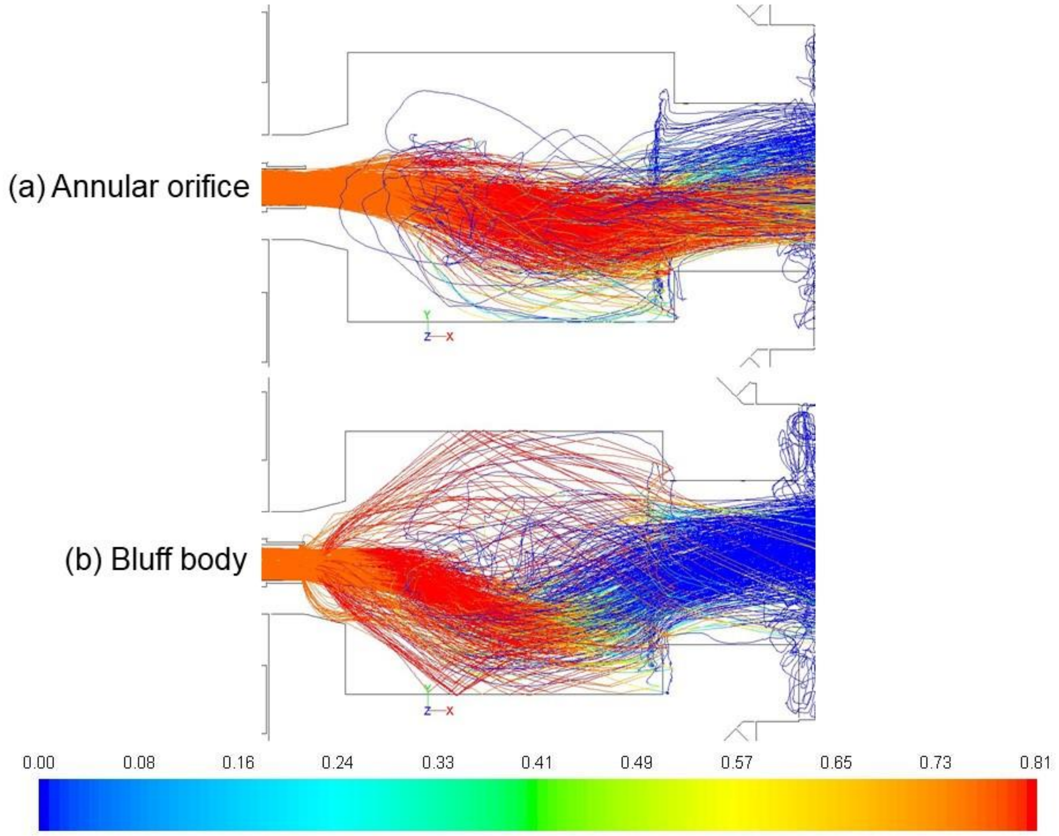

Fig. 18. Particle trajectory colored by a volatiles mass fraction inside the pre-combustion chamber for the annular orifice case (a) and the bluff body case (b)

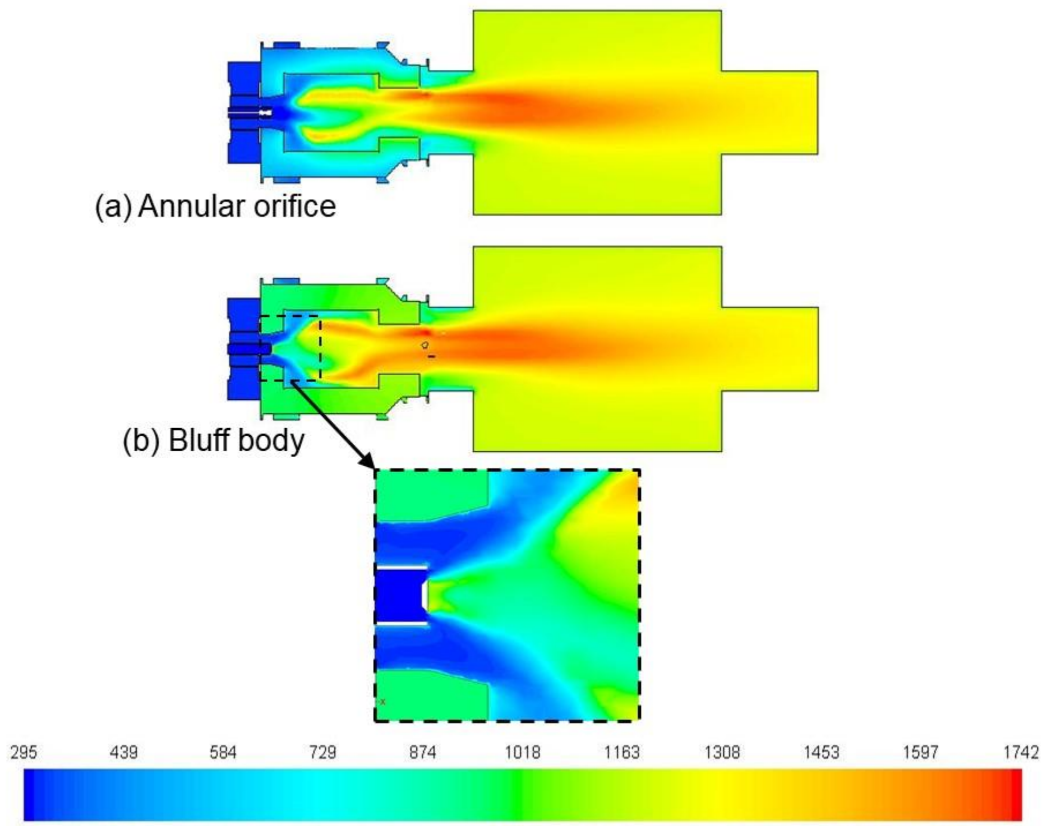

Fig. 19. Temperature (K) distribution inside the pre-combustion chamber and furnace for the annular orifice case (a) and the bluff body case (b)

Species distribution

The consumption of oxygen took place earlier in the nozzle with a bluff body. Low oxygen concentration was observed next to the burner tip (Fig. 20b). The boundary of the oxygen depletion zone was at the location where a high consumption rate took place and was defined as the location of the flame. The flame was "lifted" from the burner tip for the annular orifice case. This agrees with the flame illumination shown in Fig. 7a. As for the result with bluff body, the zone of low oxygen was found attached to the burner tip corresponding with attached flame as shown in Fig. 7b. The concentration in the main combustion chamber had decreased further, suggesting there was a greater amount of oxygen consumption. This latter case with the bluff body exhibited an earlier combustion completion than its counterpart.

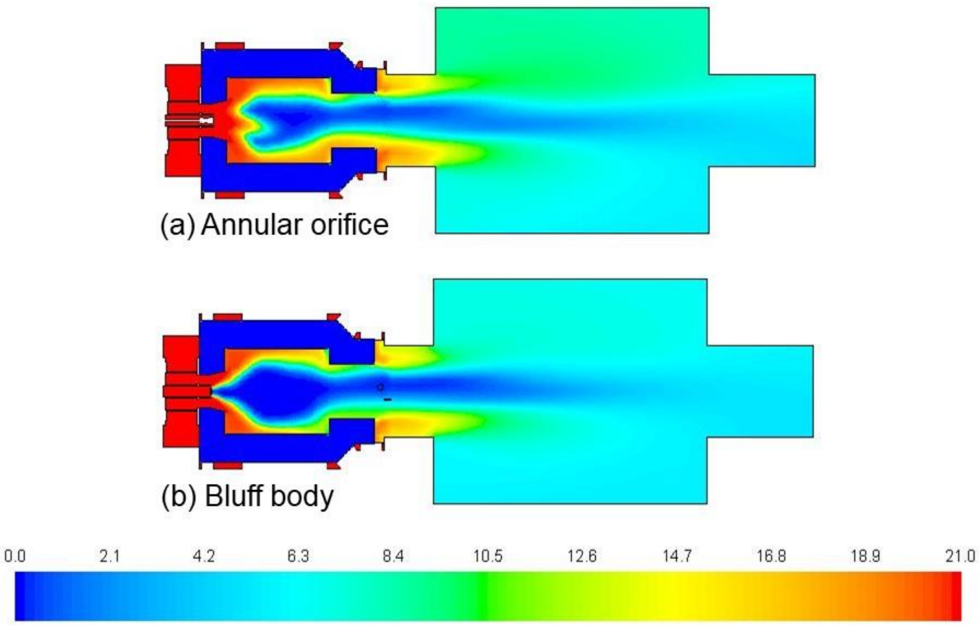

Fig. 20. O_2 concentration (vol%, dry) inside the pre-combustion chamber and furnace for the annular orifice case (a) and the bluff body case (b)

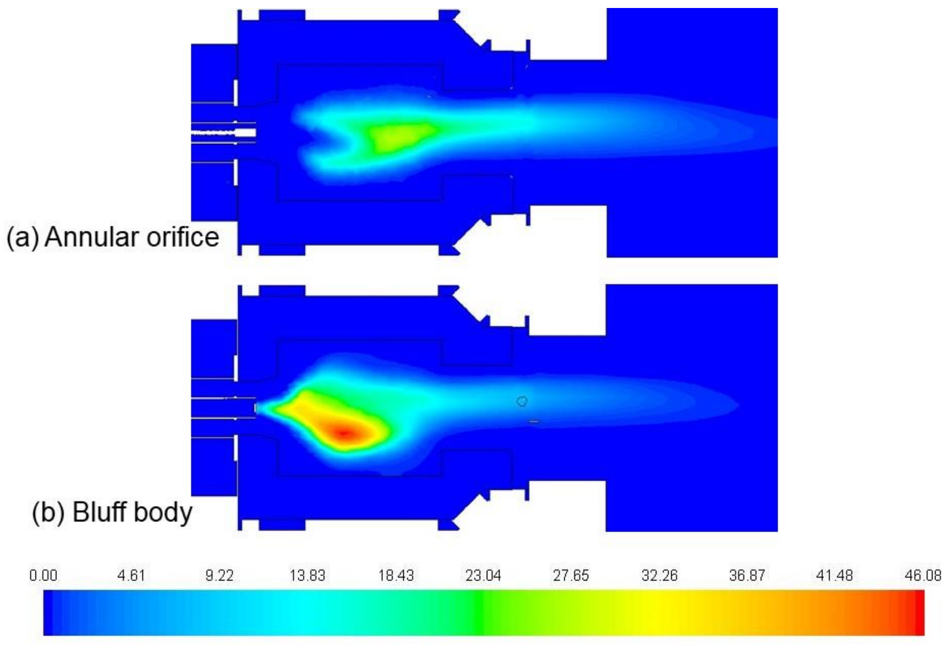

Fig. 21. Volatiles concentration (vol%, dry) inside the pre-combustion chamber and furnace for the annular orifice case (a) and the bluff body case (b)

The volatiles concentration shown in Fig. 21 has confirmed findings already discussed in an earlier section. The attachment of a high volatiles concentration zone was found in the bluff body case while the annular orifice case took place at a certain distance from the burner tip. Additionally, the concentration was higher near the center of the pre-combustion chamber. The peak value was below the centerline of the chamber because of gravitational force.

Carbon monoxide was one of the intermediate species that participates during combustion. It could have been an indication for the combustion completeness if the concentration was diminished at the exit of the furnace. As shown in Fig. 22, the bluff body provided better combustion efficiency by having an exit plane value of 241 ppm, while that of the annular orifice case was 463 ppm. This was a consequence of the greater degree of burn out when using the bluff body. The prediction resembled a trend with the results measured at the exit plane of the furnace.

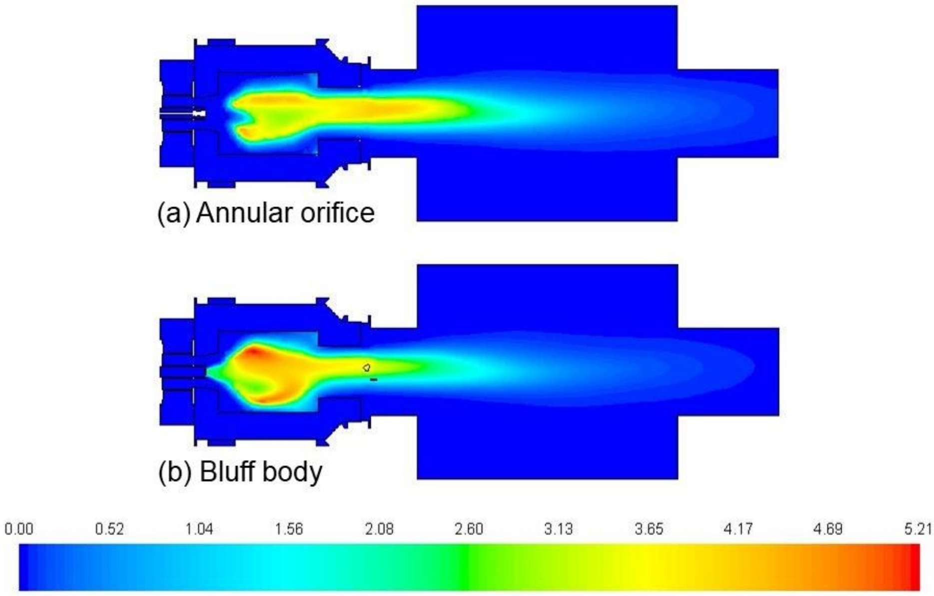

Fig. 22. CO concentration (vol%, dry) inside the pre-combustion chamber and furnace for the annular orifice case (a) and the bluff body case (b)

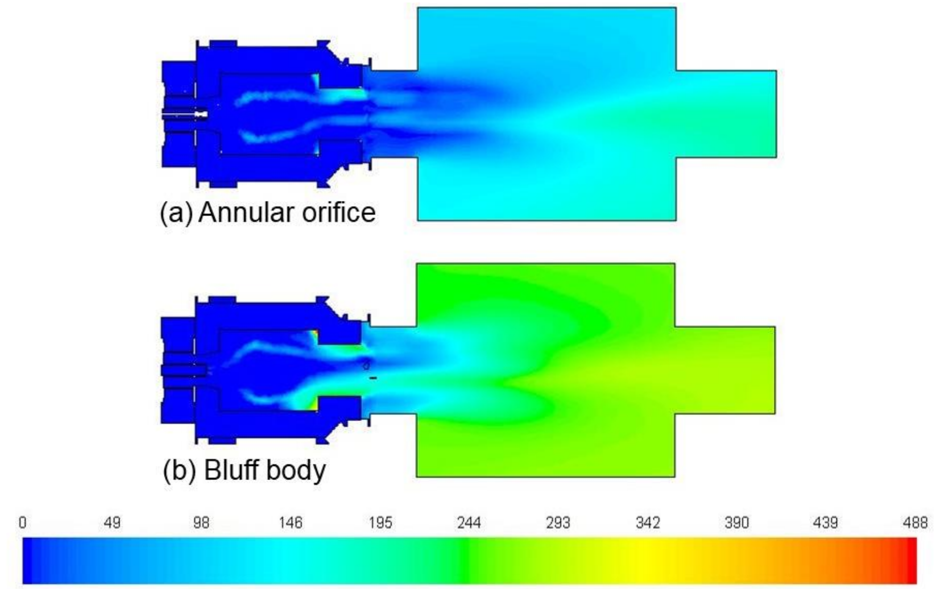

Fig. 23. NO_x concentration (ppm, dry) inside the pre-combustion chamber and furnace for the annular orifice case (a) and the bluff body case (b)

NO_x formation

The NO_x concentration is shown in Fig. 23. The formation of NO_x took place in the pre-combustion chamber and continued to form in the main furnace (Fig. 24). The peak of the NO_x source was found where the temperature was at its peak, especially at the boundary between the volatiles-rich region and the secondary air stream. This implies there was a major contribution of thermal NO_x. Prompt NO_x was additionally found with the formation rate differing by three orders of magnitude less than the thermal NO_x. The bluff body case generated a higher NO_x formation rate compared with the formation rate of the annular orifice case. This had resulted in a higher accumulation of NO_x concentration and eventually led to higher NO_x emissions at the furnace exit.

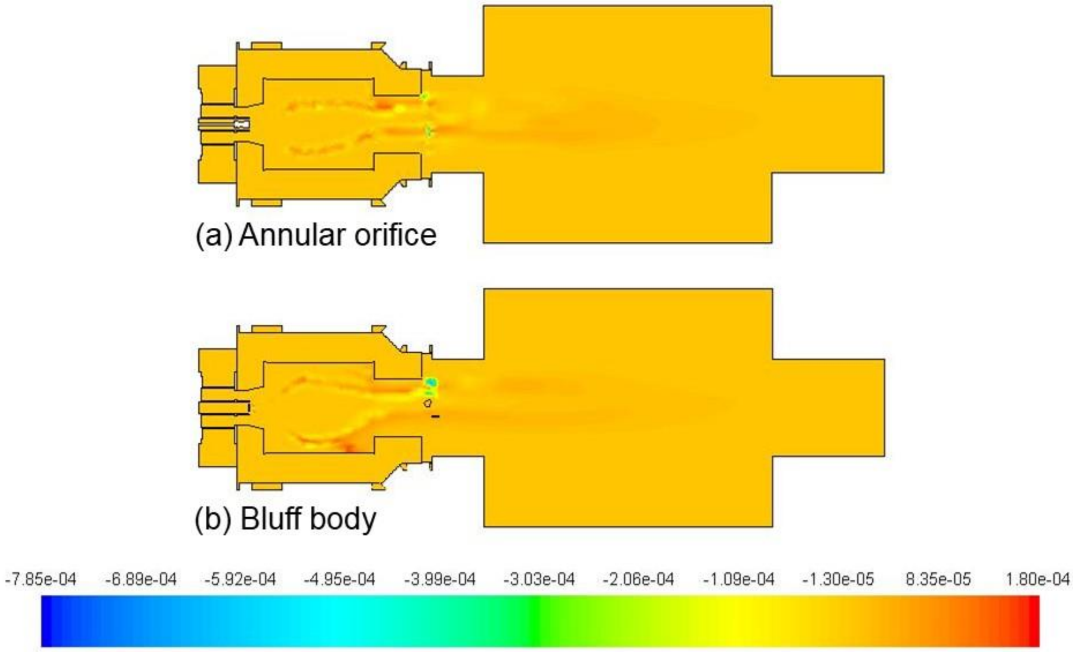

Fig. 24. Rate of NO_x (kmol/(m^3 × s)) inside the pre-combustion chamber and furnace for the annular orifice case (a) and the bluff body case (b)

CONCLUSIONS

1. In this paper, the experiment and the simulation were carried out to investigate the performance of a newly designed burner with a pre-combustion chamber firing pure pulverized biomass. The effect caused by the difference in the burner tip configuration was studied at a firing rate of 300 kW.
2. A bluff body with a blockage ratio of 0.42 of the fuel inlet nozzle, when equipped co-axially with the secondary air inlet at a swirl number of 0.83, could provide a satisfactory performance for the pure biomass combustion. It generated a sufficiently large reverse-flow zone in the pre-combustion chamber. In addition, it helped to disperse the particles away from the center of the combustion chamber, allowing for rapid heating and devolatilization.
3. With an earlier devolatilization, the ignition was attached to the burner tip. A more intense combustion was found when using the bluff body, resulting in a much higher temperature in the pre-combustion chamber compared with the annular orifice.
4. The bluff body helped the devolatilization take place almost completely within the pre-

combustion chamber, while a noticeable amount of volatiles was yet to release in the furnace in the annular orifice case. Consequently, the bluff body burner yielded a higher char burn out, a smaller amount of leftover oxygen, and a lower CO concentration at the furnace exit.

5. The NO_x emissions when installing the bluff body at the burner tip was twice as high as the annular orifice case. This observation coincided with the higher flue gas temperature in the pre-combustion chamber and the furnace, suggesting there was a contribution of thermal NO_x.

ACKNOWLEDGMENTS

The authors are grateful to the financial support from The Research and Researchers for Industries Program (RRI: PHD 57I 0045) under administration of The Thailand Research Fund.

REFERENCES CITED

Aziz, M., Budianto, D., and Oda, T. (2016). "Computational fluid dynamic analysis of co-firing of palm kernel shell and coal," *Energies* 9(3), 137. DOI: 10.3390/en9030137

Badzioch, S., and Hawksley, P. G. W. (1970). "Kinetics of thermal decomposition of pulverized coal particles," *Industrial & Engineering Chemistry Process Design and Development* 9(4), 521-530. DOI: 10.1021/i260036a005

Ballester, J., Barroso, J., Cerecedo, L. M., and Ichaso, R. (2005). "Comparative study of semi-industrial-scale flames of pulverized coals and biomass," *Combustion and Flame* 141(3), 204-215. DOI: 10.1016/j.combustflame.2005.01.005

Baum, M. M., and Street, P. J. (1971). "Predicting the combustion behaviour of coal particles," *Combustion Science and Technology* 3(5), 231-243. DOI: 10.1080/00102207108952290

Chui, E. H., and Raithby, G. D. (1993). "Computation of radiant heat transfer on a nonorthogonal mesh using the finite-volume method," *Numerical Heat Transfer, Part B: Fundamentals, An International Journal of Computation and Methodology* 23(3), 269-288. DOI: 10.1080/10407799308914901

Coppalle, A., and Vervisch, P. (1983). "The total emissivities of high-temperature flames," *Combustion and Flame* 49(1-3), 101-108. DOI: 10.1016/0010-2180(83)90154-2

Darmawan, A., Budianto, D., Aziz, M., and Tokimatsu, K. (2017). "Retrofitting existing coal power plants through cofiring with hydrothermally treated empty fruit bunch and a novel integrated system," *Applied Energy* 204, 1138-1147. DOI: 10.1016/j.apenergy.2017.03.122

De Soete, G. G. (1975) "Overall reaction rates of NO and N_2 formation from fuel nitrogen," *Symposium (International) on Combustion* 15(1), 1093-1102. DOI: 10.1016/S0082-0784(75)80374-2

Elfasakhany, A., Tao, L., Espenas, B., Larfeldt, J., and Bai, X. S. (2013). "Pulverised wood combustion in a vertical furnace: Experimental and computational analyses," *Applied Energy* 112, 454-464. DOI: 10.1016/j.apenergy.2013.04.051

Elorf, A., and Sarh, B. (2019). "Excess air ratio effects on flow and combustion characteristics of pulverized biomass (olive cake)," *Case Studies in Thermal Engineering* 13, 100367. DOI: 10.1016/j.csite.2018.100367

Fenimore, C. P. (1971). “Formation of nitric oxide in premixed hydrocarbon flames,” *Symposium (International) on Combustion* 13(1), 373-380. DOI: 10.1016/S0082-0784(71)80040-1

Field, M. A. (1969). “Rate of combustion of size-graded fractions of char from a low-rank coal between 1200 K and 2000 K,” *Combustion and Flame* 13(3), 237-252. DOI: 10.1016/0010-2180(69)90002-9

Gómez, M. A., Martín, R., Chapela, S., and Porteiro, J. (2019). “Steady CFD combustion modeling for biomass boilers: An application to the study of the exhaust gas recirculation performance,” *Energy Conversion and Management* 179, 91-103. DOI: 10.1016/j.enconman.2018.10.052

Gu, M., Zhang, M., Fan, W., Wang, L., and Tian, F. (2005). “The effect of the mixing characters of primary and secondary air on NO_x formation in a swirling pulverized coal flame,” *Fuel* 84(16), 2093-2101. DOI: 10.1016/j.fuel.2005.04.019

Kandamby, N., Lazopoulos, G., Lockwood, F. C., Perera, A., and Vigevano, L. (1996). “Mathematical modeling of NO_x emission reduction by the use of reburn technology in utility boilers,” in: *ASME Int. Joint Power Generation Conference and Exhibition*, Houston, TX.

Karim, Md. R., and Naser, J. (2018). “CFD modelling of combustion and associated emission of wet woody biomass in a 4 MW moving grate boiler,” *Fuel* 222, 656-674. DOI: 10.1016/j.fuel.2018.02.195

Launder, B. E., and Spalding, D. B. (1974). “The numerical computation of turbulent flows,” *Computer Methods in Applied Mechanics and Engineering* 3(2), 269-289. DOI: 10.1016/0045-7825(74)90029-2

Li, J., Biagini, E., Yang, W., Tognotti, L., and Blasiak, W. (2013). “Flame characteristics of pulverized torrefied-biomass combusted with high-temperature air,” *Combustion and Flame* 160(11), 2585-2594. DOI: 10.1016/j.combustflame.2013.05.010

Liu, B., Wu, Y., Cui, K., Zhang, H., Matsumoto, K., and Takeno, K. (2016). “Improvement of ignition prediction for turbulent pulverized coal combustion with EDC extinction model,” *Fuel* 181, 1265-1272. DOI: 10.1016/j.fuel.2015.12.016

Ma, L., Jones, J. M., Pourkashanian, M., and Williams, A. (2007). “Modelling the combustion of pulverized biomass in an industrial combustion test furnace,” *Fuel* 86(12-13), 1959-1965. DOI: 10.1016/j.fuel.2006.12.019

Magnussen, B. F., and Hjertager, B. H. (1977). “On mathematical modeling of turbulent combustion with special emphasis on soot formation and combustion,” *Symposium (Internat.) on Combustion* 16(1), 719-729. DOI: 10.1016/S0082-0784(77)80366-4

Murthy, J. Y., and Mathur, S. R. (1998). “Finite volume method for radiative heat transfer using unstructured meshes,” *Journal of Thermophysics and Heat Transfer* 12(3), 313-321. DOI: 10.2514/2.6363

Ndibe, C., Grathwohl, S., Paneru, M., Maier, J., and Scheftnecht, G. (2015). “Emissions reduction and deposits characteristics during cofiring of high shares of torrefied biomass in a 500 kW pulverized coal furnace,” *Fuel* 156, 177-189. DOI: 10.1016/j.fuel.2015.04.017

Pu, G., Zan, H., Du, J., and Zhang, X. (2017). “Study on NO emission in the oxy-fuel combustion of co-firing coal and biomass in a bubbling fluidized bed combustor,” *BioResources* 12(1), 1890-1902. DOI: 10.15376/biores.12.1.1890-1902

Raithby, G. D., and Chui, E. H. (1990). “A finite-volume method for predicting a radiant heat transfer in enclosures with participating media,” *Journal of Heat Transfer* 112(2), 415-423. DOI: 10.1115/1.2910394

Sami, M., Annamalai, K., and Wooldridge, M. (2001). “Co-firing of coal and biomass fuel blends,” *Progress in Energy and Combustion Science* 27(2), 171-214. DOI: 10.1016/S0360-1285(00)00020-4

Smith, T. F., Shen, Z. F., and Friedman, J. N. (1982). "Evaluation of coefficients for the weighted sum of gray gases model," *Journal of Heat Transfer* 104(4), 602-608. DOI: 10.1115/1.3245174

Wang, Y., Wang, X., Hu, Z., Li, Y., Deng, S., Niu, B., and Tan, H. (2015). "NO emissions and combustion efficiency during biomass co-firing and air-staging," *BioResources* 10(3), 3987-3998. DOI: 10.15376/biores.10.3.3987-3998

Weber, R., Poyraz, Y., Beckmann, A. M., and Brinker, S. (2015). "Combustion of biomass in jet flames," *Proceedings of the Combustion Institute* 35(3), 2749-2758. DOI: 10.1016/j.proci.2014.06.033

Yi, Q., Qi, F., Xiao, B., Hu, Z., and Liu, S. (2013). "Co-firing ramie residue with supplementary coal in a cyclone furnace," *BioResources* 8(1), 844-854. DOI: 10.15376/biores.8.1.844-854

Yin, C., Rosendahl, L., and Kær, S.K. (2012). "Towards a better understanding of biomass suspension co-firing impacts *via* investigating a coal flame and a biomass flame in a swirl-stabilized burner flow reactor under same conditions," *Fuel Processing Technology* 98, 65-73. DOI: 10.1016/j.fuproc.2012.01.024

Zeldovich, Y. B., Sadovnikov, P. Y., and Frank-Kamenetskii, D. A. (1947). *Oxidation of Nitrogen in Combustion*, Publishing House of the Acad. of Sciences of USSR, Moscow, Russia.

Zhou, L. X., Zhang, Y., and Zhang, J. (2003). "Simulation of swirling coal combustion using a full two-fluid model and an AUSM turbulence-chemistry model," *Fuel* 82(8), 1001-1007. DOI: 10.1016/S0016-2361(02)00396-4

Article submitted: March 5, 2019; Peer review completed: May 25, 2019; Revised version received and accepted: June 6, 2019; Published: June 17, 2019.
DOI: 10.15376/biores.14.3.6146-6167